*American Mineralogist, Volume 97, pages 1662–1669, 2012*

# Semi-quantitative determination of the Fe/Mg ratio in synthetic cordierite using Raman spectroscopy‡

**Udo Haefeker,* Reinhard Kaindl,† and Peter Tropper**

Institute of Mineralogy and Petrography, University Innsbruck, Innrain 52, A-6020 Innsbruck, Austria

## Abstract

Investigations of $H_2O$-bearing synthetic well-ordered Mg-Fe-cordierites ($X_{Fe}$ = 0–1) with micro-Raman spectroscopy revealed a linear correlation between the Fe/Mg ratio and the position of certain Raman peaks. In the range between 100 and 1250 $cm^{-1}$, all peaks except for three peaks shift toward lower wavenumbers with increasing $X_{Fe}$ as a consequence of the substitution of the lighter Mg by the heavier Fe atom on the octahedral sites and the associated structural changes. Selected medium and strong peaks show a shift of 5 to 13 $cm^{-1}$, respectively. Based on recent quantum-mechanical calculations (Kaindl et al. 2011) these shifts can be attributed to specific vibrational modes in the cordierite structure, thus showing that the Mg-Fe exchange affects the vibrational modes of tetrahedral, octahedral, and mixed sites. The peaks (wavenumber Mg-/Fe-cordierite) at 122/111, 262/257, 430/418, 579/571, 974/967, and 1012/1007 $cm^{-1}$ were selected for detailed deconvolution analysis. The shifts of these peaks were then plotted vs. $X_{Fe}$ and regression of the data lead to the formulation of a set of linear equations. Assuming ideal Fe-Mg mixing of the end-members and using linear peak shifts then allows the development of calibration diagrams for the semi-quantitative determination of the Fe-Mg contents of cordierite samples with Raman spectroscopy. In addition, the effect of different $H_2O$ contents and the degree of Al-Si ordering on the Fe/Mg determination were also investigated. Testing the calibration against data from six well-characterized natural cordierite samples yielded excellent agreement.

**Keywords:** Raman spectroscopy, cordierite, Mg-Fe exchange, peak shift, Al-Si ordering

## Introduction

The Mg-Fe silicate cordierite with the idealized formula $(Mg,Fe)_2Al_4Si_5O_{18}\cdot nH_2O$ occurs as hexagonal high-temperature and orthorhombic low-temperature polymorphs with disordered/ordered Al-Si distribution on the tetrahedral sites. Cordierite is an important petrogenetic mineral because, when in equilibrium with other Mg-Fe-silicates, the Mg/Fe ratio of cordierite can be used as a geothermobarometer (e.g., Lonker 1981; Bhattacharya 1986; Kalt et al. 1999; Kalt 2000). Various amounts of volatiles like $H_2O$ and $CO_2$ can also be incorporated into the structural channels of cordierite, which allows paleofluid reconstructions (Harley et al. 2002; Bul'bak and Shvedenkov 2005; Rigby et al. 2008). Most of the natural cordierites are fully ordered and have the space group symmetry *Cccm*. Structurally, six-membered rings of $(Si,Al)O_4$ are stacked along the crystallographic *c*-axis and form channels, laterally and vertically linked by additional (Al, Si) tetrahedrons. The octahedral coordinated M sites, two different tetrahedral coordinated T sites ($T_1$, $T_2$) and the channel sites (Ch0, Ch1/4) are distinguished in the structure, according to the general formula:

$$(M)_2(T_11)_2(T_26)_2(T_23)_2(T_21)_2(T_16)O_{18}(Ch0,Ch1/4)$$

where Si occupies the $T_23$, $T_21$, and $T_16$ sites and Al the remaining two $T_11$ and $T_26$ sites. Structural refinement and Al/Si-ordering was investigated by various authors (e.g., Gibbs 1966; Langer and Schreyer 1969; Meagher and Gibbs 1977; Cohen et al. 1977; Hochella et al. 1979; Putnis 1980; Wallace and Wenk 1980; Putnis and Bish 1983; Armbruster 1985; Malcherek et al. 2001; Bertoldi et al. 2004 and references therein; Miletich et al. 2010). The Mg and $Fe^{2+}$ ions are located in the octahedral coordinated M sites and their mixing is assumed to be ideal (e.g., Boberski and Schreyer 1990); 90 to 99% $Fe^{2+}$ occupies the octahedral site (Khomenko et al. 2001). The amount of $Fe^{3+}$ in natural cordierites is insignificantly low (Geiger et al. 2000). The incorporation of $Fe^{2+}$ in exchange for Mg leads to multiple structural changes: (1) expansion of the mean M-O-distances within the octahedra leads to the elongation of the unit cell in **a**- and **b**-directions and (2) $T_11$-O distances decrease slightly, leading to a contraction along the *c*-axis (e.g., Wallace and Wenk 1980; Armbruster 1985; Boberski and Schreyer 1990; Malcherek et al. 2001; Geiger and Grams 2003). Raman and Fourier transform infrared (FTIR) spectroscopic methods were already used by several authors to investigate and describe different properties of cordierite, like polymorphism (Langer and Schreyer 1969), volatile content (Vry et al. 1990; Kalt 2000; Kolesov and Geiger 2000; Yakubovich

* E-mail: udo.haefeker@uibk.ac.at

† Present address: MATERIALS, Institute for Surface Technologies and Photonics, Functional Surfaces, JOANNEUM RESEARCH Forschungsgesellschaft mbH, Leobner Strasse 94, A-8712 Niklasdorf, Austria.

‡ Open Access, thanks to the authors' funding. Article available to all readers via GSW (http://ammin.geoscienceworld.org) and the MSA web site.

et al. 2004; Bul'bak and Shvedenkov 2005; Khomenko and Langer 2005; Kaindl et al. 2006; Kolesov 2006; Nasdala et al. 2006; Rigby et al. 2008; Weikusat et al. 2010), Al-Si ordering (McMillan et al. 1984; Güttler et al. 1989; Poon et al. 1990), structural heterogeneity and energetic and structural changes under high pressure (Geiger and Grams 2003; Likhacheva et al. 2011). Local structural heterogeneities in natural Fe-Mg-cordierites and their thermodynamic mixing properties have also been investigated with IR spectroscopy (Geiger and Grams 2003). Quantum-mechanical calculations of the Raman spectra of Mg- and Fe-cordierites have also been done for a detailed peak assignment and a theoretical description of the effects of the Mg-Fe exchange and Al-Si ordering (Kaindl et al. 2011). Semi-quantitative techniques for the determination of chemical compositions, based on the shifts of vibrational modes within certain mineral solid solutions, have been presented for example for garnets, olivines, and pyroxenes (Geiger and Grams 2003; Smith 2005; Kuebler et al. 2006; Bersani et al. 2009; Stalder et al. 2009). The aim of this work is the detailed Raman spectroscopic description of structural changes in $H_2O$-bearing synthetic cordierite as a consequence of Mg-Fe-exchange and the development of semi-quantitative calibrations for the determination of the Mg/Fe ratio in natural and synthetic cordierite samples.

## Experimental methods

### Synthesis of Mg-Fe-cordierites and sample preparation

Cordierites with the composition $(Mg,Fe)_2Al_4Si_5O_{18}\cdot nH_2O$ were synthesized using annealing and hydrothermal techniques. $SiO_2$ nanopowder (99.5%, metals basis, Aldrich), $Al_2O_3$ (γ, 99,997%, metals basis, Alfa Aesar), MgO (Art. 5865, Merck), FeO [Iron (II) oxide, 99.5%, metals basis, Alfa Aesar], Fe (Art. 3819, Merck), and graphite powder were used for the synthesis. The synthesis of the hydrous Fe- and the dry Mg-end-member has been described in detail by Kaindl et al. (2011). To obtain $H_2O$-bearing samples, orthorhombic Mg-cordierite was treated hydrothermally in a welded gold capsule together with $H_2O$ at 700 °C and 0.2 GPa for 7 days. The full synthesis sequence was: stoichiometric glass → nucleation/formation of "β-cordierite" → disordered hexagonal anhydrous cordierite → ordered orthorhombic anhydrous cordierite → ordered orthorhombic hydrous cordierite. The transition from hexagonal to orthorhombic Mg-cordierite caused the formation of a patchy "tweed" microstructure in the cordierite crystals (Putnis 1983; Armbruster 1985; Putnis et al. 1987; Blackburn and Salje 1999).

Powdered glass with Mg-cordierite stoichiometry and the oxides FeO, $Al_2O_3$, and $SiO_2$ in various fractions were used as starting material for the synthesis of hydrous cordierite crystals with $X_{Fe}$ [=Fe/(Fe + Mg)] ranging from 0.1 to 0.4. Sealed buffered double capsules were then used, with IW (iron/wüstite) buffer and $H_2O$ in the outer gold-capsule and the starting material and $H_2O$ in an inner $Ag_{70}Pd_{30}$ capsule. The experimental conditions were 700 °C and 0.2 GPa and the experimental duration was 7 days. For the synthesis of hydrous crystals with $X_{Fe}$ = 0.5–0.8 cordierite glasses with $X_{Fe}$ = 0.5–0.8 were produced. The glasses were then tempered in a welded gold capsule together with graphite powder for 16 to 24 h at 900 °C to obtain the unordered hexagonal cordierite. This cordierite was then loaded together with $H_2O$ in a hydrothermal apparatus at 700 °C and 0.25–0.3 GPa for 7 days to obtain well-ordered $H_2O$-bearing orthorhombic cordierite. The syntheses were done in buffered capsules with IW-buffer and $H_2O$ in the outer gold capsules and the starting material and $H_2O$ in the inner $Ag_{70}Pd_{30}$ capsules.

### Electron microprobe analysis

For electron microprobe analyses (EMPA), all synthesis products were embedded in an epoxy mount, grinded, and finally polished using a 1 µm diamond suspension. The orientation of the crystals from run products was random. The JEOL JXA 8100 Superprobe at the Institute of Mineralogy and Petrography at the University of Innsbruck was used for the chemical analyses of the glasses, the intermediate run products and the final cordierite samples. Analytical conditions for the wavelength dispersive measurements were 15 kV acceleration voltage and a beam current of 10 nA. Counting times for all elements were 20 s for the peak and 10 s for the background. For the calibration synthetic (corundum) and natural (almandine, quartz, orthoclase, and diopside) microprobe standards were used. Mineral formulas were calculated on an anhydrous basis of 18 O atoms. Some measurements were performed in point mode due to the small grain size and inhomogeneities in the synthesis materials. Depending on the elements and their concentrations the standard deviation of the measurements of each element is between 0.34 and 1.79%. For precise correlation we used backscattered electron (BSE) imaging to correlate the locations of the analyzed spots with the locations of the subsequent Raman spectroscopic investigations.

### X-ray powder diffraction

Powder X-ray diffraction (XRD) for the determination of the lattice parameters and the degree of Al-Si ordering in the Mg-cordierite samples was done with a Stoe STADI-MP diffractometer system in bisecting transmission geometry in a 2Θ range from 2 to 129.8° in steps of 0.009°. The system is equipped with a "Mythen" 1k detector and an asymmetric Ge(111)-monochromator yielding a strictly monochromatic Cu$K\alpha_1$ radiation. For the Fe-end-member a Bruker D8 Discover system with Bragg-Brentano-geometry over a 2Θ range from 5 to 80.25° in steps of 0.009° was used. The system is equipped with a copper target and a silicon-strip-detector. Rietveld calculations and LeBail fits were done using the program FullProf (Rodriguez-Carvajal 2011). The background was determined by linear interpolation between a set of breakpoints with refineable heights. Intensities within 10 times the full-width at half maximum (FWHM) of a peak were considered to contribute to the central reflection. Thompson-Cox-Hastings pseudo-Voigt functions were chosen for the simulation of the peak shape, including an asymmetry correction following Finger et al. (1994).

For the hydrous orthorhombic Mg-end-member the cell parameters are: $a$ = 17.055, $b$ = 9.724, $c$ = 9.348, and a distortion index (Miyashiro 1957) of ~0.24. The cell dimensions of the hydrous orthorhombic Fe-end-member are: $a$ = 17.244, $b$ = 9.828, $c$ = 9.288 and the distortion index is ~0.24.

### Raman spectroscopy

Due to small grain sizes and the patchy microstructure of synthetic cordierite all measurements were done on randomly oriented crystals. Unpolarized and polarized spectra of synthetic cordierite crystals were measured on a Labram HR-800 confocal Raman-spectrometer by HORIBA, using the 532 nm excitation wavelength of a 30 mW Nd:YAG laser through a 100× objective with a numerical aperture of 0.9. The size and power of the laser spot on the surface was approximately 1 µm and 5 mW, respectively. The confocal pinhole aperture was 1000 µm and the width of the entrance slit 100 µm. A grating with 1800 lines/mm was used to disperse the scattered Raman light, which was detected by an open-electrode charge-coupled device with 1024 × 256 pixels, each with a size of 43 µm. The spectral resolution of 1.4 $cm^{-1}$ was determined by measuring the Rayleigh line. Accuracy of the Raman line shifts was checked by regular measurements of the emission lines of a Ne spectral calibration lamp and the deviation was ±0.24 $cm^{-1}$. Background and Raman peaks were fitted using the built-in spectrometer software LabSpec with the line-segments baseline correction and convoluted Gauss-Lorentz functions. The spectra were recorded for 2 × 200 s in the area of 100–1250 $cm^{-1}$ using unpolarized (no additional polarizers used) and polarized laser light (polarizers were used for excitation and the scattered Raman light). Deconvolution is not trivial since the spectra of cordierite are characterized by (1) complex peak overlaps forming band systems (envelopes) and by (2) peak broadening in Fe-rich samples. In the unpolarized spectra most of the band systems are dominated by intense peaks and cordierite shows a strong spectroscopic anisotropy. While peak intensities strongly depend on the orientation of the crystal to the polarization plane of the laser light, there are, however, no orientation effects of the peak positions. The contribution of individual peaks to the band system varies with the overall orientation of the crystal thus influencing band shapes and positions. For the determination of individual peaks and their positions within the band systems, each sample was measured twice using polarized laser light for excitation and a polarizer for the scattered light set perpendicular and parallel to the laser polarization. This filtering-procedure was necessary for a successful deconvolution process because removing specific peaks within complex band systems facilitates the identification of others. In addition, the area between 100 and 350 $cm^{-1}$, which shows a higher peak density, was measured for 2 × 200 s in a high-resolution mode with an entrance slit set to 20 µm. The sub-pixel acquisition function was then used to increase the peak definition by providing five-times more data points. The information gained from the detailed measurements was used together with the calculated peak positions by Kaindl et al. (2011) thus providing the initial values for the deconvolution of the band systems. Multi-peak fitting with simultaneous and stepwise fitting of several narrow peaks

was necessary for the more complex band systems (Bradley 2007; Knorr 2011). The errors of the deconvolution process were determined empirically by repeating the curve-fit routine for all six peaks of Fe-cordierite used in the calibration diagrams in an unpolarized spectrum 10 times. The Fe-end-member was selected because the effect of peak-broadening and peak-overlapping is higher compared to Mg-bearing cordierites. For the calibration the peak position of the unpolarized and polarized measurements were used. Detailed chemical analyses and descriptions of the investigated natural cordierite samples can be found in Bertoldi et al. (2004).

## Results

### Mg-cordierite

The Raman spectra of 16 randomly oriented cordierite samples with compositions from $X_{Fe}$ = 0 to 1 were investigated between 100 and 1250 cm$^{-1}$. Characteristic for the Raman spectra of Mg-Fe-cordierites are regions with dominant peaks and band systems containing various numbers of overlapping peaks, which show a diagnostic shift toward lower wavenumbers with increasing Fe-contents. Exceptions are the low-intensity bands around 330, 909, and 960 cm$^{-1}$. After a close investigation of the Raman spectra of all available samples in different orientations we selected six peaks, which seemed to be most suitable for the development of a calibration curve because of their accessibility in terms of intensities, orientation effects, and peak shift values (Fig. 1). In Mg-cordierite these are medium- to high-intensity peaks at 121 cm$^{-1}$ (A), 261.5 cm$^{-1}$ (B), 430 cm$^{-1}$ (C), 579 cm$^{-1}$ (D), 974 cm$^{-1}$ (E), and 1012.5 cm$^{-1}$ (F). The peak at 121 cm$^{-1}$ is the dominant peak in the complex band system in the region from 100 to 135 cm$^{-1}$. Toward lower wavenumbers there are medium- to low-intensity peaks at 118 and 116 cm$^{-1}$. Adjacent to a small gap between 114 and 109 cm$^{-1}$, a low-intensity peak follows at 107 cm$^{-1}$. Toward higher wavenumbers, the peak at 121 cm$^{-1}$ is strongly overlapped by a second intense peak at 123 cm$^{-1}$, followed by medium- to high-intensity peaks at 126, 129, and 131 cm$^{-1}$.

The peak at 261.5 cm$^{-1}$ is the most intense peak in the band system in the region 230 to 275 cm$^{-1}$, which contains 8 individual peaks. Toward lower wavenumbers this peak is overlapped by a high-intensity peak at 260 cm$^{-1}$ followed by a low-intensity peak at 256 cm$^{-1}$. A group of three medium- to low-intensity peaks follows at 243, 242, and 241 cm$^{-1}$. Toward higher wavenumbers the 261.5 cm$^{-1}$ peak is overlapped by medium- to low-intensity peaks at 265 and 269 cm$^{-1}$. The medium-intensity peak at 430 cm$^{-1}$ is flanked by a low-intensity peak at 436 cm$^{-1}$.

The high-intensity peak at 579 cm$^{-1}$ is part of a band system with 5 individual peaks. Toward lower wavenumbers it is overlapped by the medium-intensity peak at 566 cm$^{-1}$ and a high-intensity peak at 557 cm$^{-1}$, followed by a low-intensity peak at 546 cm$^{-1}$. Toward higher wavenumbers this peak is overlapped by a low-intensity peak at 592 cm$^{-1}$. The high-intensity peak at 974 cm$^{-1}$ has a neighboring peak at 952 cm$^{-1}$ with medium intensity. The medium- to high-intensity peak follows at 1012.5 cm$^{-1}$.

The experimental data are in good agreement with the calculated cordierite Raman spectra by Kaindl et al. (2011), which allow the unambiguous assignment of the peaks A–E. According to Kaindl et al. (2011) peak A results from the modes deforming and rotating mainly the $T_1$6 site. Peak B results from the bending modes of both the Si- and Al-tetrahedral and the M-octahedral sites. Peak C is a result from the bending of the $T_2$6 site. The split bands between 500 and 630 cm$^{-1}$ including band (D) are related to the bending vibrations of the $T_2$6, $T_2$1, and $T_2$3 and the stretching of the M and $T_2$6 sites. Peak E is caused by the stretching of the $T_2$1 and $T_1$6 sites. Peak F is caused by the stretching of the $T_2$1 and $T_2$3 ring-tetrahedra as well as the $T_1$6 tetrahedron, which connects two M sites. A complete band assignment for both cordierite Fe- and Mg-end-members can be found in Kaindl et al. (2011).

### Fe-cordierite and peak shifts

In the spectra of the Fe-end-member, the equivalent peaks can be found at 110.5 cm$^{-1}$ (A´), 256.5 cm$^{-1}$ (B´), 418 cm$^{-1}$ (C´), 571.5 cm$^{-1}$ (D´), 967 cm$^{-1}$ (E´), and 1007.5 cm$^{-1}$ (F´). Figure 2

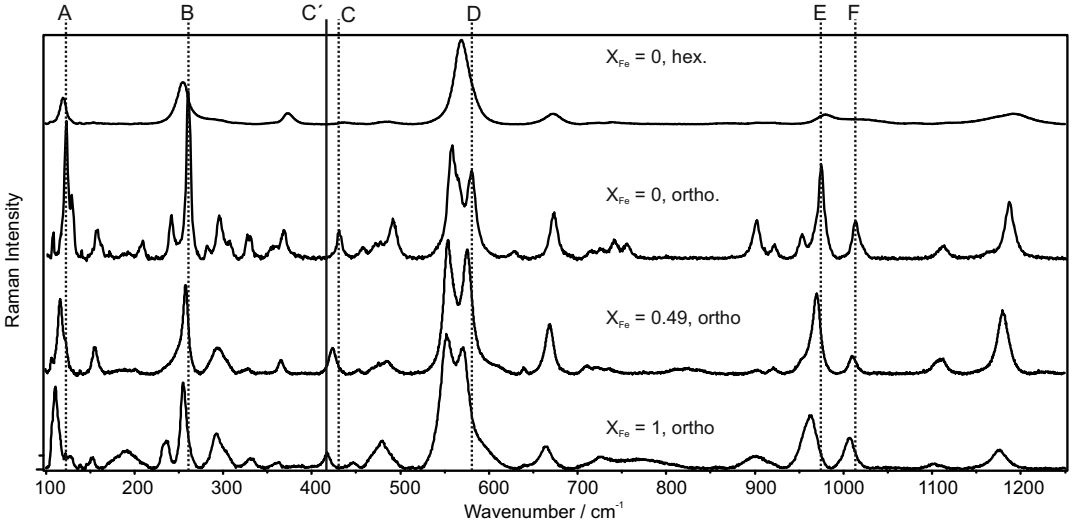


**Figure 1.** Unpolarized Raman spectra of disordered, hexagonal (**top**), and ordered, orthorhombic modifications (**bottom**) of Mg-Fe-cordierite with $X_{Fe}$ = 0, 0.49, and 1 over the range of 100–1250 cm$^{-1}$. The positions of the peaks A–F in Mg-cordierite are indicated by vertical stippled lines. The position of C´ is indicated by a vertical solid line.

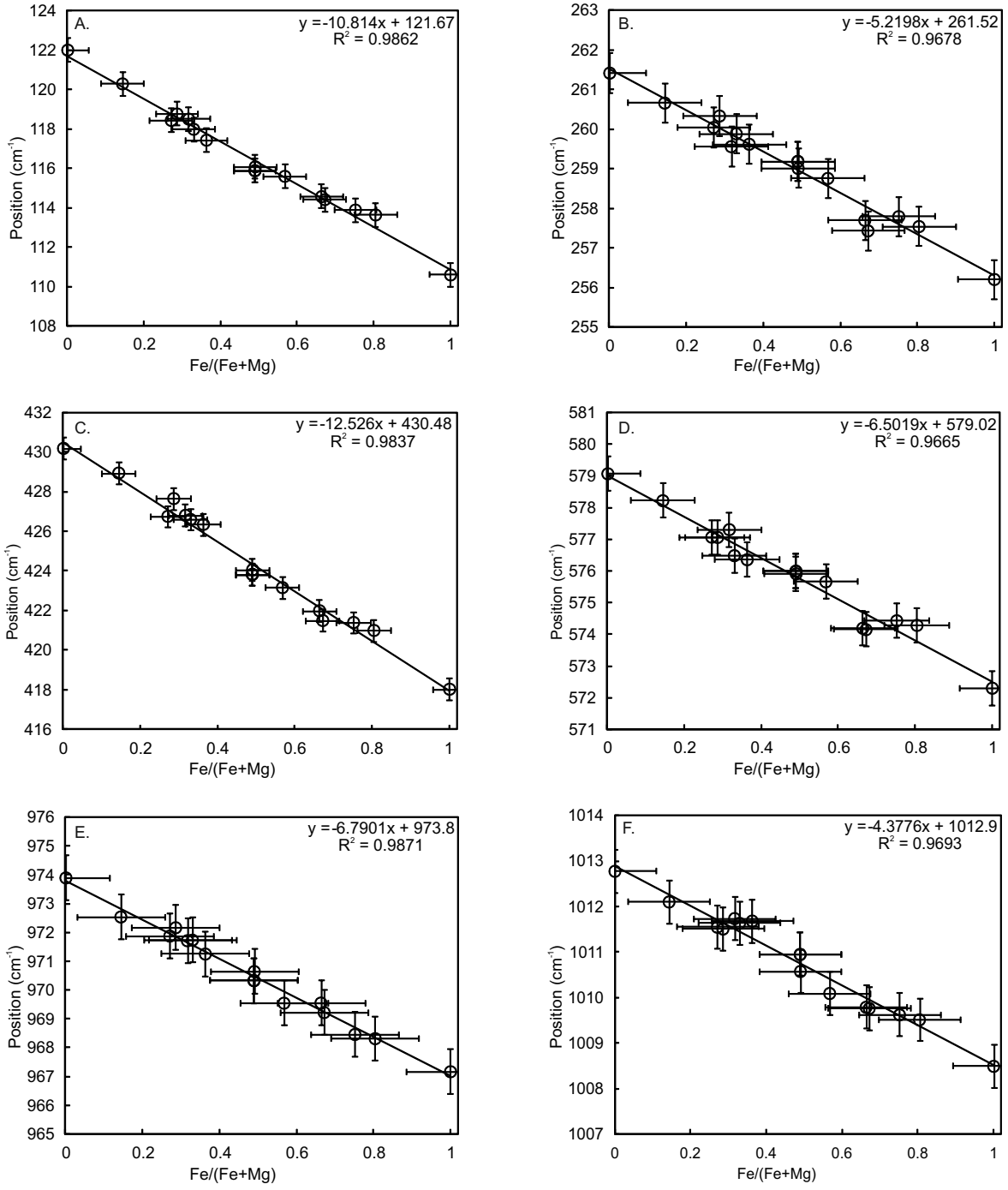


**FIGURE 2. (a–f)** Resulting calibration diagrams. The diagrams show the peak shift of the peaks A–F toward lower wavenumbers as a function of Fe/(Fe + Mg) based on the samples listed in Table 1. The error bars show the maximum 2σ standard deviations (calculated for the Fe-end-member).

shows the peak shifts as a function of the Fe-content for the 16 samples listed in Table 1. Peaks A/A′ and C/C′ show the highest shifts with 11 and 12 $cm^{-1}$, whereas peaks B/B′ and E/E′ show the lowest shifts with 5 $cm^{-1}$.

Regressions of the data of peaks A–F lead to the following linear equations:

$$\text{(A)}\ X_{\mathrm{Fe}} = \frac{P_{(A)} - 121.67}{-10.814}$$

$$\text{(B)}\ X_{\mathrm{Fe}} = \frac{P_{(B)} - 261.52}{-5.2198}$$

**TABLE 1.** Electron microprobe analysis of 16 synthetic hydrous cordierite samples

| Sample | 1 | 2 | 3 | 4 | 5 | 6 | 7 | 8 |
|---|---|---|---|---|---|---|---|---|
| Name | 12.5h_7 | 33.4_5 | 33.4_2 | 33.4_6 | 33.7.2_2.2 | 33.7.2_5 | 33.7.2_2.1 | 29.2_1 |
| $SiO_2$ | 50.03(36) | 48.61(33) | 48.72(33) | 48.43(33) | 48.60(33) | 47.73(32) | 47.71(32) | 48.92(34) |
| $Al_2O_3$ | 33.82(28) | 32.94(26) | 33.64(26) | 33.36(26) | 32.13(26) | 32.84(26) | 33.03(26) | 31.96(26) |
| FeO | n.d. | 3.48(12) | 6.00(16) | 6.40(16) | 7.44(17) | 7.62(18) | 8.21(18) | 11.34(22) |
| MgO | 13.85(21) | 11.67(17) | 9.08(15) | 8.98(15) | 9.03(15) | 8.72(15) | 8.08(14) | 6.64(14) |
| Total | 97.70(50) | 96.70(47) | 97.44(47) | 97.17(47) | 97.20(48) | 96.91(47) | 97.03(47) | 98.86(50) |
| Si | 4.988(36) | 4.978(34) | 4.998(34) | 4.993(34) | 5.037(34) | 4.969(34) | 4.972(34) | 5.069(36) |
| Al | 3.975(33) | 3.976(32) | 4.068(32) | 4.054(32) | 3.924(31) | 4.030(32) | 4.057(32) | 3.903(32) |
| Fe | n.d. | 0.298(11) | 0.515(13) | 0.552(14) | 0.645(15) | 0.663(15) | 0.715(16) | 0.982(19) |
| Mg | 2.058(31) | 1.781(26) | 1.389(23) | 1.38(23) | 1.395(24) | 1.353(23) | 1.255(23) | 1.025(22) |
| $X_{Fe}$ | 0.00 | 0.14 | 0.27 | 0.29 | 0.32 | 0.33 | 0.36 | 0.49 |
| Sample | 9 | 10 | 11 | 12 | 13 | 14 | 15 | 16 |
| Name | 30.1B1_2 | 29.2_3 | 29.2_2 | 31.2_6r | 31.2_5r | 37_1-3 | 38 | 26.5_8 |
| $SiO_2$ | 48.26(34) | 47.9(34) | 47.86(34) | 45.16(32) | 44.99(32) | 47.45(25) | 46.44(24) | 45.96(32) |
| $Al_2O_3$ | 32.36(27) | 31.73(26) | 31.66(26) | 32.53(26) | 32.26(26) | 32.25(20) | 30.84(20) | 30.64(25) |
| FeO | 11.25(21) | 12.47(22) | 13.18(23) | 14.23(24) | 14.46(24) | 16.65(36) | 17.68(37) | 21.09(29) |
| MgO | 6.57(14) | 5.33(13) | 4.82(12) | 4.05(11) | 3.97(11) | 3.04(08) | 2.42(07) | n.d. |
| Total | 98.44(50) | 97.43(50) | 97.52(50) | 95.97(49) | 95.68(49) | 99.39(49) | 97.38(49) | 97.69(50) |
| Si | 5.023(35) | 5.063(35) | 5.070(36) | 4.904(34) | 4.907(34) | 5.011(26) | 5.034(26) | 5.053(35) |
| Al | 3.97(33) | 3.954(32) | 3.953(32) | 4.163(33) | 4.147(33) | 4.037(25) | 3.95(25) | 3.97(33) |
| Fe | 0.979(19) | 1.102(20) | 1.168(21) | 1.292(21) | 1.319(22) | 1.491(32) | 1.613(34) | 1.94(26) |
| Mg | 1.019(21) | 0.841(20) | 0.762(19) | 0.656(18) | 0.645(17) | 0.498(12) | 0.402(11) | n.d. |
| $X_{Fe}$ | 0.49 | 0.57 | 0.61 | 0.66 | 0.67 | 0.75 | 0.80 | 1.00 |

*Note*: The chemical formulas are normalized to 18 O atoms; $X_{Fe}$ = Fe/(Fe + Mg); n.d.: not detected. The numbers in parentheses are 2σ standard deviations in terms of the last two digits.

$$\text{(C)}\ X_{\text{Fe}} = \frac{P_{(C)} - 430.48}{-12.526}$$

$$\text{(D)}\ X_{\text{Fe}} = \frac{P_{(D)} - 579.02}{-6.5019}$$

$$\text{(E)}\ X_{\text{Fe}} = \frac{P_{(E)} - 973.8}{-6.7901}$$

$$\text{(F)}\ X_{\text{Fe}} = \frac{P_{(F)} - 1012.9}{-4.3776}.$$

The standard deviations $2\sigma_1$ (hardware uncertainties) and $2\sigma_2$ (fitting procedures) for the Raman positions were calculated with Equation 1, the overall standard deviations $2\sigma_{\text{overall}}$ were calculated with Equation 2

$$\sigma_{1,2} = \sqrt{\frac{\sum\left(x - \bar{x}\right)^2}{\left(n-1\right)}} \quad (1)$$

$$\sigma_{\text{overall}} = \sqrt{\sigma_1^2 + \sigma_2^2}. \quad (2)$$

The 2σ standard deviations are given in Figures 2a–2f. The calculations based on a spectrum of Fe-cordierite yielded a significantly higher error in the peak position and thus in the prediction of $X_{Fe}$ due to the uncertainties using spectral curve fitting procedures compared to Mg-cordierite.

## DISCUSSION

### Peak shifts and structural changes in Mg-Fe-cordierite

The general trend of downshift of peaks in Fe-cordierite compared to their equivalents in Mg-cordierite is probably caused by decreasing mean M-O and increasing $T_1$1-O bond distances (Malcherek et al. 2001). However, for individual peaks the interplay seems to be extremely complex: The equivalent peaks C/C′ for example result both from vibrations of Al in the $T_2$6 site. Peak A in Mg-cordierite is assigned to Si in the $T_1$6, $T_2$1, and $T_2$3 sites, whereas peak A′ in Fe-cordierite is assigned to Al in the $T_1$1 site and Fe in the M site (Kaindl et al. 2011). This complexity is reflected in the larger number of Gauss-Lorentz functions necessary to deconvolute peaks A/A′. Furthermore, one has to take into account the limited accuracy of peak assignments by quantum mechanical calculations (up to ±16 $cm^{-1}$ for individual peaks), substitutions of Mg and $Fe^{2+}$ for Al and compositional dependence of Al-Si ordering (Malcherek et al. 2001; Kaindl et al. 2011). Further discussion is therefore restricted to the practical aspects of the observed dependencies between peak shifts and Fe-contents.

### Influences on the Raman measurements I: The effects of Al-Si ordering and $H_2O$ content

Natural Mg-Fe-cordierites are mainly orthorhombic with a fully ordered Al/Si distribution on the tetrahedral sites and distortion indices (Miyashiro 1957) between 0.21 and 0.27 (e.g., Hochella et al. 1979; Armbruster and Bloss 1981). Since the disordered hexagonal polymorph (distortion index 0) occurs as an intermediate phase in the annealing experiments and was used as starting material for some of the hydrothermal experiments, it was necessary to reinvestigate the effect of Al/Si ordering on the Raman peak positions, mainly because the distortion indices of our synthetically grown hydrous cordierites do not exceed values of ~0.245. The hexagonal to orthorhombic transition and related changes in the Raman spectra (Fig. 1) can be described with an increase of the number of Raman active modes from 10 to 33, peak sharpening accompanied by intensity increase and the simultaneous splitting of the strong band at 567 $cm^{-1}$ into three bands at 557, 564, and 578 $cm^{-1}$ (McMillan et al.1984; Poon et al.

1990). Kaindl et al. (2011) calculated five modes in this energy region for the ordered orthorhombic polymorph. Al-Si ordering in synthetic annealed cordierite is a function of temperature and time (Putnis and Bish 1983; McMillan et al. 1984). While longer annealing times at temperatures of 1200 °C result in increasing distortion indices, the Raman spectra of cordierites do not change significantly after the transition from hexagonal to orthorhombic symmetry. The spectra of orthorhombic cordierite samples with annealing times of 3 and 348 h at 1400 °C show no significant differences of the peak positions in the area between 100 and 1250 $cm^{-1}$; only the split band at ~557 $cm^{-1}$ shows a small shift of <1 $cm^{-1}$ toward lower wavenumbers.

The hydrothermal experiments with glass or disordered cordierite as starting material have shown that (1) the ordering process depends of the amount of $H_2O$ present in the capsule during the hydrothermal synthesis at relatively low temperatures of 700 °C. Experiments with no or very low amounts of $H_2O$ available show no or only low degrees of Al-Si ordering. (2) The size of the starting material also has an effect on the ordering process. Figures 3a and 3b show Raman data at the rim of a hydrothermally treated, stoichiometric Fe-cordierite glass fragment with a size of several hundred micrometers. The split peak region between 500 and 650 $cm^{-1}$ and the intensities of the $H_2O$ peak around 3600 $cm^{-1}$ are shown across a distance of 80 µm from the rim into the interior. The amount of $H_2O$ incorporated and the peak-splitting distance decrease with increasing distance to the fluid contact zone at the outer rim. The profiles suggest a maximum penetration depth limit of water of about 20 µm.

Investigations of anhydrous and hydrous orthorhombic Mg-cordierite confirm that $H_2O$ incorporation does not affect the position of the Raman peaks except for one peak at ~1180 $cm^{-1}$, which shifts toward lower wavenumbers with increasing $H_2O$ contents. Therefore, this peak was excluded for Mg-Fe determination since the amount of $H_2O$ in the channels of natural cordierites is variable (e.g., Bertoldi et al. 2004).

### Influences on the Raman measurements II: The nature of the starting materials

Some of the EMPA of Fe-rich samples gave low totals of 95.68–97.50 wt%. All of the synthetic cordierites used in this study contain water but the amount of channel $H_2O$ is insufficient to explain these deviations. A possible reason could be the presence of $Fe^{3+}$ within the structure, which was not considered in mineral formula calculations. Attempts for $Fe^{3+}$ determinations with Mössbauer-spectroscopy failed due to a lack of a sufficient amount of sample material.

EMPA showed that the synthesis products of our Mg-Fe-experiments are in some cases inhomogeneous with variations of $\pm X_{Fe} \leq 0.08$ within the same capsule. We assume that the short synthesis times prevented pervasive equilibration within the capsules. To avoid further uncertainties related to inhomogeneous compositions in the intermediate Fe-Mg range structural data with powder XRD were only collected for the homogeneous Fe- and Mg-end-members.

High-resolution Raman investigations of the region 100–135 $cm^{-1}$ of Mg-cordierite reveal a higher peak density than expected since quantum-mechanical calculations by Kaindl et al. (2011) predicted six peaks, but the experimental data show at least eight individual peaks in this area. This might result from an imperfect cordierite structure with defects and/or distortions, activating otherwise forbidden bands due to breaking of selection rules. Such theoretically forbidden bands have been observed for example in halides, borosilicate feldspar, zeolites, silica glasses, dodecaborides, and $GeO_2$ (Benedek and Nardelli 1967; Bäuerle 1973; Best et al. 1994; Mihailova et al. 2005; Nesterova et al. 2005; Werheit et al. 2011; Kaindl et al. 2012).

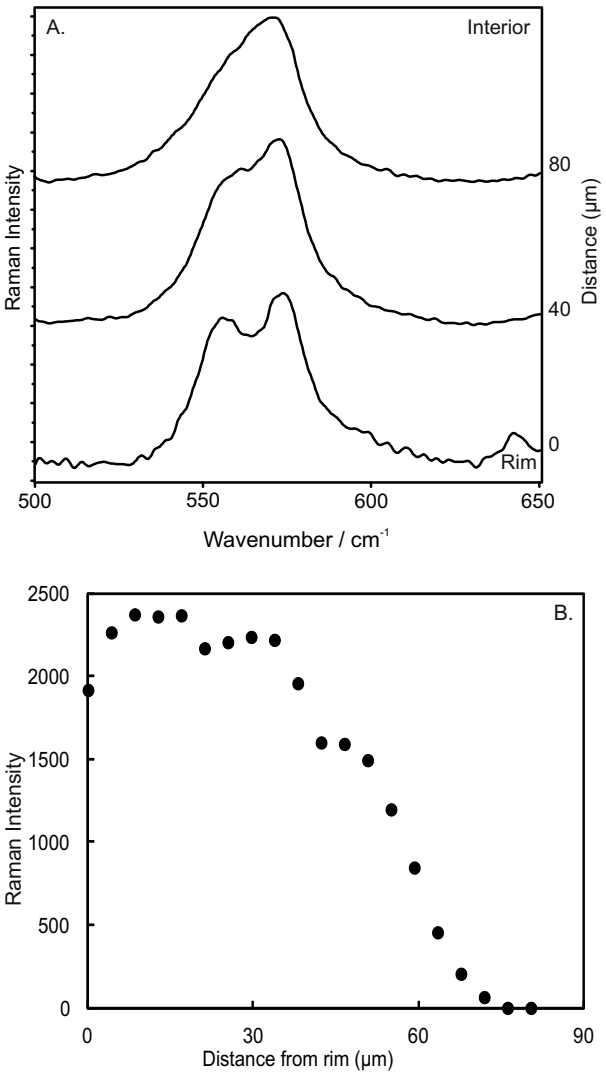


**Figure 3.** (**a** and **b**) The figures show the splitting of the peaks in the area of 575 $cm^{-1}$ as a consequence of Al-Si ordering in Fe-cordierite (**a**) and the intensities of the type-1 water peak at 3597 $cm^{-1}$ (**b**) over a distance of 80 µm from the rim toward the interior of the crystal.

### Application of the calibration to natural samples

All of the presented correlation diagrams (Figs. 2a–2f) can be used for semi-quantitative determinations of $X_{Fe}$ in natural samples. The main difficulty when working with Raman spectra of cordierites are peak-overlaps and hence the precise determination of individual peak positions. For practical purposes and to reduce the errors introduced by the fitting procedures, we

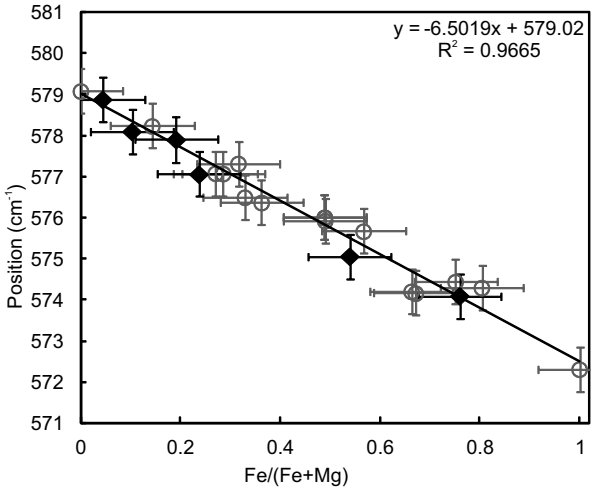


**FIGURE 4.** Raman shift of band D. The open circles represent the data as a function of $X_{Fe}$. The black line is the linear regression to the data. Six natural cordierite samples from Bertoldi et al. (2004) with $X_{Fe}$ 0.04–0.76 (black diamonds) are also shown in the diagram. The error bars show the maximum 2σ standard deviations (calculated for the Fe-end-member).

recommend the use of calibration diagrams (Figures) 2c, 2d, 2e, and 2f, although the correlation coefficients of all six regression equations are close to 1. Band deconvolution of these peaks is less complex and time consuming; the other diagrams (Figs. 2a and 2b) can be used when the results are inconsistent or higher precision is necessary. The complexity of the two band systems in the region 100–350 $cm^{-1}$ is a potential source of error during the de-convolution process.

Figure 4 shows a calibration diagram based upon peak D at 575 $cm^{-1}$. The obtained peak positions of six natural well-characterized cordierite samples were added to the diagram and are in good agreement with the experimental data. The Fe-Mg composition of the samples TA-1 with $X_{Fe} = 0.04$, WYO-2 with $X_{Fe} = 0.10$, C005 with $X_{Fe} = 0.19$, VS3 with $X_{Fe} = 0.24$, HO6 with $X_{Fe} = 0.54$ and TUB-1 with $X_{Fe} = 0.76$ could be adequately reproduced by the Raman technique presented here. The good reproducibility of these natural samples also shows that chemical deviations from the ideal stoichiometric composition have no effect on the measurements thus far. The natural samples contain minor amounts of Mn, Be, Li, and Zn as well as channel cations and volatiles (Na, K, $CO_2$).

The good agreement of $X_{Fe}$ derived by independent methods and Raman spectroscopy confirms that incorporation of these components influences the cordierite structure to a much lesser extent than Fe-Mg exchange and Si-Al order-disorder.

## ACKNOWLEDGMENTS

We thank Martina Tribus for her help with the EMPA, Jürgen Konzett for the valuable advice with respect to the experiments, and Daniel Többens for his help with powder XRD analysis. This study was funded by the Austrian Science Fund (FWF): [P22013-N21].

## REFERENCES CITED

Armbruster, T. (1985) Crystal structure refinement, Si, Al-ordering, and twinning in "Pseudo-hexagonal" Mg-cordierite. Neues Jahrbuch für Mineralogie Monatshefte, 255–267.

Armbruster, T. and Bloss, F.D. (1981) Mg-Cordierite: Si/Al ordering, optical properties, and distortion. Contributions to Mineralogy and Petrology, 77, 332–336.

Bäuerle, D. (1973) Vibrational spectra of electron and hydrogen centers in ionic crystals. Springer Tracts in Modern Physics, 68, 76–160.

Benedek, G. and Nardelli, G.F. (1967) Raman scattering by color centers. Physical Review, 154, 872–876.

Bersani, D., Andò, S., Vignola, P., Moltifiori, G., Marino, I.-G., Lottici, P.P., and Diella, V. (2009) Micro-Raman spectroscopy as a routine tool for garnet analysis. Spectrochimica Acta Part A, 73, 484–491.

Bertoldi, C., Proyer, A., Garbe-Schönberg, D., Behrens, H., and Dachs, E. (2004) Comprehensive chemical analyses of natural cordierites: implications for exchange mechanisms. Lithos, 78, 389–409.

Best, S.P., Clark, R.J.H., Hayward, C.L., and Withnall, R. (1994) Polarized single-crystal Raman spectroscopy of danburite, $CaB_2Si_2O_8$. Journal of Raman Spectroscopy, 25, 557–563.

Bhattacharya, A. (1986) Some geobarometers involving cordierite in the FeO-$Al_2O_3$-$SiO_2$ (±$H_2O$) system: refinements, thermodynamic calibration, and applicability in granulite-facies rocks. Contributions to Mineralogy and Petrology, 94, 387–394.

Blackburn, J.F. and Salje, K.H. (1999) Sandwich domain walls in cordierite: a computer simulation study. Journal of Physics: Condensed Matter, 11, 4747–4766.

Boberski, C. and Schreyer, W. (1990) Synthesis and water contents of $Fe^{2+}$-bearing cordierites. European Journal of Mineralogy, 2, 565–584.

Bradley, M. (2007) Curve Fitting in Raman and IR Spectroscopy: Basic Theory of Line Shapes and Applications. Thermo Fisher Scientific, Madison, U.S.A., Application Note: 50733.

Bul'bak, T.A. and Shvedenkov, G.Yu. (2005) Experimental study on incorporation of C-H-O-N fluid components in Mg-cordierite. European Journal of Mineralogy, 17, 829–838.

Cohen, J.P., Ross, F.K., and Gibbs, G.V. (1977) An X-ray and neutron diffraction study of hydrous low cordierite. American Mineralogist, 62, 67–78.

Finger, L.W., Cox, D.E., and Jephcoat, A.P. (1994) A correction for powder diffraction peak asymmetry due to axial divergence. Journal of Applied Crystallography, 27, 892–900.

Geiger, C.A. and Grams, M. (2003) Cordierite IV: structural heterogeneity and energetics of Mg–Fe solid solutions. Contributions to Mineralogy and Petrology, 145, 752–764.

Geiger, C.A., Rager, H., and Czank, M. (2000) Cordierite III: the site occupation and concentration of Fe3+. Contributions to Mineralogy and Petrology, 140, 344–352.

Gibbs, G.V. (1966) The polymorphism in cordierite I: the crystal structure of low cordierite. American Mineralogist, 51, 1068–1087.

Güttler, B., Salje, E., and Putnis, A. (1989) Structural states of Mg cordierite III: Infrared spectroscopy and the nature of the hexagonal-modulated transition. Physics and Chemistry of Minerals, 16, 365–373.

Harley, S.L., Thompson, P., Hensen, B.J., and Buick, I.S. (2002) Cordierite as a sensor of fluid conditions in high-grade metamorphism and crustal anatexis. Journal of Metamorphic Geology, 20, 71–86.

Hochella, M.F., Brown, G.E., Ross, F.K., and Gibbs, G.V. (1979) High-temperature crystal chemistry of hydrous Mg- and Fe-cordierites. American Mineralogist, 64, 337–351.

Kaindl, R., Tropper, P., and Deibl, I. (2006) A semi-quantitative technique for determination of $CO_2$ in cordierite by Raman spectroscopy in thin sections. European Journal of Mineralogy, 18, 331–335.

Kaindl, R., Többens, D., and Haefeker, U. (2011) Quantum-mechanical clculations of the Raman spectra of Mg- and Fe-cordierite. American Mineralogist, 96, 1568–1574.

Kaindl, R., Többens, D., Penner, S., Bielz, T., Soisuwan, S., and Klötzer, B. (2012) Quantum mechanical calculations of the vibrational spectra of the quartz- and rutile-type $GeO_2$. Physics and Chemistry of Minerals, 39, 47–55.

Kalt, A. (2000) Cordierite channel volatiles as evidence for dehydration melting: an example from high-temperature metapelites of the Bayerische Wald (Variscan belt, Germany). European Journal of Mineralogy, 12, 987–998.

Kalt, A., Berger, A., and Blümel, P. (1999) Metamorphic evolution of cordierite-bearing migmatites from the Bayerische Wald (Variscan Belt, Germany). Journal of Petrology, 40, 601–627.

Khomenko, V.M. and Langer, K. (2005) Carbon oxides in cordierite channels: Determination of $CO_2$ isotopic species and CO by single crystal IR spectroscopy. American Mineralogist, 90, 1913–1917.

Khomenko, V.M., Langer, K., and Geiger, C. (2001) Structural locations of the iron ions in cordierite. Contributions to Mineralogy and Petrology, 141, 381–396.

Knorr, B.M. (2011) Examples in Peak Fitting. Seminar in Modern Physics. Department of Physics, Lehigh University, Bethlehem, Pennsylvania.

Kolesov, B.A. (2006) Raman spectra of single $H_2O$ molecules isolated in cavities of crystals. Journal of Structural Chemistry, 47, 21–34.

Kolesov, B.A. and Geiger, C.A. (2000) Cordierite II: The role of $CO_2$ and $H_2O$.

American Mineralogist, 85, 1265–1274.
Kuebler, K.E., Jolliff, B.L., Wang, A., and Haskin, L.A. (2006) Extracting olivine (Fo-Fa) compositions from Raman spectral peak positions. Geochimica et Cosmochimica Acta, 70, 6201–6222.
Langer, K. and Schreyer, W. (1969) Infrared and powder X-ray diffraction studies on the polymorphism of cordierite, $Mg_2(Al_4Si_5O_{18})$. American Mineralogist, 54, 1442–1459.
Likhacheva, A.Y., Goryainov, S.V., Krylov, A.S., Bul'bak, T.A., and Prasad, S.R. (2012) Raman spectroscopy of natural cordierite at high water pressure up to 5 GPa. Journal of Raman Spectroscopy, 43, 559–563.
Lonker, S.W. (1981) The *P-T-X* relations of the cordierite-garnet-sillimanite-quartz equilibrium. American Journal of Science, 63, 1056–1090.
Malcherek, T., Domeneghetti, M.C., Tazzoli, V., Ottolini, L., McCammon, C., and Carpenter, A. (2001) Structural properties of ferromagnesian cordierites. American Mineralogist, 86, 66–79.
McMillan, P., Putnis, A., and Carpenter, M.A. (1984) A Raman-spectroscopic study of Al-Si ordering in synthetic magnesium cordierite. Physics and Chemistry of Minerals, 10, 256–260.
Meagher, E.P. and Gibbs, G.V. (1977) The polymorphism of cordierite II: The crystal structure of indialite. Canadian Mineralogist, 15, 43–49.
Mihailova, B., Valtchev, V., Mintova, S., Faust, A.C., Petkov, N., and Bein, T. (2005) Interlayer stacking disorder in zeolite beta family: a Raman spectroscopic study. Physical Chemistry Chemical Physics, 7, 2756–2763.
Miletich, R., Gatta, G.D., Redhammer, G.J., Burchard, M., Meyer, H.P., Weikusat, C., Rotiroti, N., Glasmacher, U.A., Trautmann, C., and Neumann, R. (2010) Structure alterations in microporous $(Mg,Fe)_2Al_4Si_5O_{18}$ crystals induced by energetic heavy-ion irradiation. Journal of Solid State Chemistry, 183, 2372–2381.
Miyashiro, A. (1957) Cordierite-indialite relations. American Journal of Sciences, 255, 43–62.
Nasdala, L., Wildner, M., Wirth, R., Groschopf, N., Pal, D.C., and Möller, A. (2006) Alpha particle haloes in chlorite and cordierite. Mineralogy and Petrology, 86, 1–27.
Nesterova, Z.V., Melo Melchor, G., and Alexandrov, I.V. (2005) Medium-range ordering in glass structures as a background of photosensitivity in silica fibers. Journal of Non-Crystalline Solids, 351, 3789–3796.
Poon, W.C.K., Putnis, A., and Salje, E. (1990) Structural states of Mg cordierite: IV. Raman spectroscopy and local order parameter behavior. Journal of Physics: Condensed Matter, 2, 6361–6372.
Putnis, A. (1980) Order-modulated structures and the thermodynamics of cordierite reactions. Nature, 287, 128–131.
Putnis, A. and Bish, D.L. (1983) The mechanism and kinetics of Al, Si ordering in Mg-cordierite. American Mineralogist, 68, 60–65.
Putnis, A., Salje, E., Redfern, S.A.T., Fyfe, C.A., and Strobl, H. (1987) Structural states of Mg-cordierite I: Order parameters from synchrotron X-ray and NMR data. Physics and Chemistry of Minerals, 14, 446–454.
Rigby, M.J., Droop, G.T.R., and Bromiley, G.D. (2008) Variations in fluid activity across the Etive thermal aureole, Scotland: evidence from cordierite volatile contents. Journal of Metamorphic Geology, 26, 331–346.
Rodriguez-Carvajal, J. (2011) FullProf. 2k, ver. 5.20. Institut Laue-Langevin, Grenoble, France.
Smith, D.C. (2005) The RAMANITA© method for non-destructive and in situ semi-quantitative chemical analysis of mineral solid-solutions by multidimensional calibration of Raman wave number shifts. Spectrochimica Acta Part A, 61, 2299–2314.
Stalder, R., Kronz, A., and Schmidt, B.C. (2009) Raman spectroscopy of synthetic $(Mg,Fe)SiO_3$ single crystals. An analytical tool for natural orthopyroxenes. European Journal of Mineralogy, 21, 27–32.
Vry, J.K., Brown, P.E., and Valley, J.W. (1990) Cordierite volatile content and the role of $CO_2$ in high-grade metamorphism. American Mineralogist, 75, 71–88.
Wallace, J.H. and Wenk, H.R. (1980) Structure variation in low cordierites. American Mineralogist, 65, 96–111.
Weikusat, C., Miletich, R., Glasmacher, U.A., Trautmann, C., and Neumann, R. (2010) Heavy-ion irradiation on crystallographically oriented cordierite and the conversion of molecular $CO_2$ to CO: a Raman spectroscopic study. Physics and Chemistry of Minerals, 37, 417–424.
Werheit, H., Filipov, V., Shirai, K., Dekura, H., Shitsevalova, N., Schwarz, U., and Armbruster, M. (2011) Raman scattering and isotopic phonon effects in dodecaborides. Journal of Physics: Condensed Matter, 23, 065403, 26 p.
Yakubovich, O.V., Massa, V., Pekov, I.V., Gavrilenko, P.G., and Chukanov, N.V. (2004) Crystal Structure of the Na-, Ca-, Be-cordierite and crystallochemical regularities in the cordierite-sekaninaite series. Crystallography Reports, 49, 953–963.

Manuscript received April 5, 2012
Manuscript accepted July 4, 2012
Manuscript handled by G. Diego Gatta